

Brownian ratchets driven by asymmetric nucleation of hydrolysis waves

Amit Lakhanpal and Tom Chou

Dept. of Biomathematics & Dept. of Mathematics, UCLA, Los Angeles, CA 90095-1766

(Dated: March 13, 2022)

We propose a stochastic process wherein molecular transport is mediated by asymmetric nucleation of domains on a one-dimensional substrate. Track-driven mechanisms of molecular transport arise in biophysical applications such as Holliday junction positioning and collagenase processivity. In contrast to molecular motors that hydrolyze nucleotide triphosphates and undergo a local molecular conformational change, we show that asymmetric nucleation of hydrolysis waves on a track can also result in directed motion of an attached particle. Asymmetrically cooperative kinetics between “hydrolyzed” and “unhydrolyzed” states on each lattice site generate moving domain walls that push a particle sitting on the track. We use a novel fluctuating-frame, finite-segment mean field theory to accurately compute steady-state velocities of the driven particle and to discover parameter regimes which yield maximal domain wall flux, leading to optimal particle drift.

PACS numbers: 82.39.-k, 87.16.Ac, 05.40.-a

Molecular motors such as kinesins, myosins, helicases, and polymerases typically convert part of the free energy of ATP or GTP hydrolysis to a conformational change [1]. This molecular deformation leads to motion of the motor against a load on a track. Although the literature on such molecular motors is vast, much less attention has been paid to the theory of molecular motions that exploit the dynamics of the track on which translation occurs. Such loads are propelled by the track, which itself is undergoing catalyzed state changes by, *e.g.*, hydrolysis.

Two biological strategies involving track-propelled particles are collagenase catalysis and Holliday junction transport. Collagenase MMP-1, an enzyme that associates with and cleaves collagen, is propelled by proteolysis of the collagen track [2, 3]. The cleaving of bonds prevents the collagenase from diffusing back across the broken bond, resulting in biased transport of the collagenase. Thus the statistical dynamics of the track propels the enzyme. This dynamic has been modeled by a burnt bridge model [3, 4, 5, 6].

Another system where substrate modification possibly leads to biased motion is the translocation of Holliday junctions [7]. The Holliday junction at which two double-stranded DNA molecules exchange one of their strands may be moved by the dynamics of hydrolysis states of the DNA binding protein RecA. RecA polymerizes on at least one of the strand-exchanging dsDNA molecules, assembling into a long nucleoprotein filament. The RecA monomers appear to hydrolyze ATP and can exist in different states, much like the intermediate hydrolysis states of myosin motors. The dynamics of the interconversion among these hydrolysis states may provide the force necessary to rotate DNA strands about each other during Holliday junction translocation. An especially promising model of this process exploits asymmetric cooperativity in the hydrolysis of the nucleotide triphosphate cofactors associated with each RecA monomer. This intrinsic asymmetry of the filament gives rise to “waves” of hydrolyzed monomers with a preferred direction, thereby moving the junction by virtue of its preferential attachment to the hydrolyzed segment of the RecA filament [7]. These examples constitute only two of many mechanisms through which chemical energy may be harnessed to perform mechanical work by the substrate rather than a motor protein. In this Letter, we develop a general stochastic theory of track-driven, hydrolysis wave-mediated transport. In addition to analyzing our model using Monte-Carlo (MC) simulations, we also formulate a moving-frame mean field theory (MFT) that accurately predicts novel features of the transport.

As in models of the ATP cycle of myosin motors, in RecA hydrolysis wave-mediated transport the RecA subunits can exist in a number of substates corresponding to sites that have bound ATP, ADP+P_i, ADP, or are empty. To simplify our model, we will assume that each site of the substrate lattice exists in only one of two possible states, “hydrolyzed” ($\sigma = 1$) and “unhydrolyzed” ($\sigma = 0$). Any lattice site i can transition from state $\sigma_i = 1$ to state $\sigma_i = 0$ with rate k_0 . The reverse process, physically corresponding to “hydrolysis” or “nucleation,” fills an empty site. In our model, an asymmetry arises in the nucleation transitions $\sigma_i = 0 \rightarrow \sigma_i = 1$. If site $i - 1$ is also in the state $\sigma_{i-1} = 0$, then the transition $\sigma_i = 0 \rightarrow \sigma_i = 1$ occurs with rate k_- . However, if

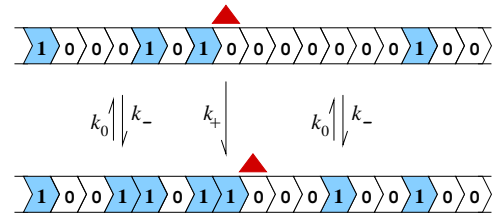


FIG. 1: Schematic of the asymmetric nucleation process. An intrinsic asymmetry in the lattice sites gives rise to asymmetric cooperativity and nucleation. The transported particle is represented by a triangle.

As in models of the ATP cycle of myosin motors, in RecA hydrolysis wave-mediated transport the RecA subunits can exist in a number of substates corresponding to sites that have bound ATP, ADP+P_i, ADP, or are empty. To simplify our model, we will assume that each site of the substrate lattice exists in only one of two possible states, “hydrolyzed” ($\sigma = 1$) and “unhydrolyzed” ($\sigma = 0$). Any lattice site i can transition from state $\sigma_i = 1$ to state $\sigma_i = 0$ with rate k_0 . The reverse process, physically corresponding to “hydrolysis” or “nucleation,” fills an empty site. In our model, an asymmetry arises in the nucleation transitions $\sigma_i = 0 \rightarrow \sigma_i = 1$. If site $i - 1$ is also in the state $\sigma_{i-1} = 0$, then the transition $\sigma_i = 0 \rightarrow \sigma_i = 1$ occurs with rate k_- . However, if

$\sigma_{i-1} = 1$, then the transition $\sigma_i = 0 \rightarrow \sigma_i = 1$ occurs with rate k_+ . If $k_+ \neq k_-$, the process is asymmetric and can lead to a steady-state current of domain walls. If a particle is associated with the lattice, it will be pushed each time a domain wall passes it. Thus, a net flux of domain walls will lead to directed particle transport. The kinetics of the lattice is outlined in Fig. 1.

The corresponding Master equation is similar to that which describes Glauber dynamics of a one-dimensional Ising model, except that the asymmetry in the transition rates prevents this system from supporting an equilibrium state. Since no exact solutions are known, we employ a hybrid finite-segment mean field theory (MFT) and MC simulations to obtain quantitative results and physical understanding.

First consider a translationally invariant (infinite or periodic) lattice in the absence of an associated load particle. In the fixed laboratory frame, the moments $\langle \sigma_i \sigma_j \dots \rangle$ of the hydrolysis states can be derived from the Master equation. These hierarchical moment equations are not closed. For example, the equation for the first moment

$$\frac{d\langle \sigma_i \rangle}{dt} = k_- - (k_- + k_0)\langle \sigma_i \rangle + \Delta\langle \sigma_{i-1} \rangle - \Delta\langle \sigma_i \sigma_{i-1} \rangle, \quad (1)$$

where $\Delta \equiv k_+ - k_-$ is the hydrolysis asymmetry, depends on correlations $\langle \sigma_i \sigma_{i-1} \rangle$. The simplest mean field approximation assumes $\langle \sigma_i \sigma_{i-1} \rangle = \langle \sigma_{i-1} \rangle \langle \sigma_i \rangle$, which, when combined with the steady-state limit ($d\langle \sigma_i \rangle / dt = 0$) of Eq. 1 gives a steady-state mean hydrolysis level

$$\langle \sigma_i \rangle = \frac{k_+ - 2k_- - k_0}{2\Delta} + \frac{\sqrt{(k_+ - k_0)^2 + 4k_- k_0}}{2\Delta}. \quad (2)$$

As shown by the dotted curves in Fig. 2a, this result is only in qualitative agreement with the mean hydrolysis level obtained from MC simulations on a lattice with $N = 1000$ sites (open circles).

The locality of the asymmetric interactions suggests that correlations are short-ranged as in the totally asymmetric exclusion process [8, 9]. Thus, more accurate approximations can be systematically implemented by considering small clusters in which all possible configurations are identified, and enumerating all the transitions among them. The densities at both ends of this cluster are then self-consistently matched to bulk values inferred by the statistics within the cluster. This finite-segment mean field approach has been used to study the nonequilibrium steady-states of related models such as the asymmetric exclusion process [10, 11]. For example, consider all possible configurations in a segment of $m = 2$ lattice sites. If we enumerate the states corresponding to the binary representation of the state number, (*i.e.*, $P_0 = 00, P_1 = 01, P_2 = 10, P_3 = 11$), the $2^2 \times 2^2$ transition matrix defined by $\dot{\mathbf{P}} = \mathbf{M}\mathbf{P}$ is

$$\mathbf{M} = \begin{bmatrix} -2k_- - s\Delta & k_0 & k_0 & 0 \\ k_- & -k_0 - k_- - s\Delta & 0 & k_0 \\ k_- + s\Delta & 0 & -k_+ - k_0 & k_0 \\ 0 & k_- + s\Delta & k_+ & -2k_0 \end{bmatrix}, \quad (3)$$

where $\mathbf{P} = (P_0, P_1, P_2, P_3)^T$ is the probability vector and s is the mean occupancy of the site immediately to the left of the explicitly enumerated pair. Since s represents the mean occupation of the rightmost site of the preceding segment, we impose self-consistency by setting $\sum_{i=\text{odd}} P_i = s$ and solving for s numerically. The simple mean field approximation (Eq. 2) corresponds to $m = 1$.

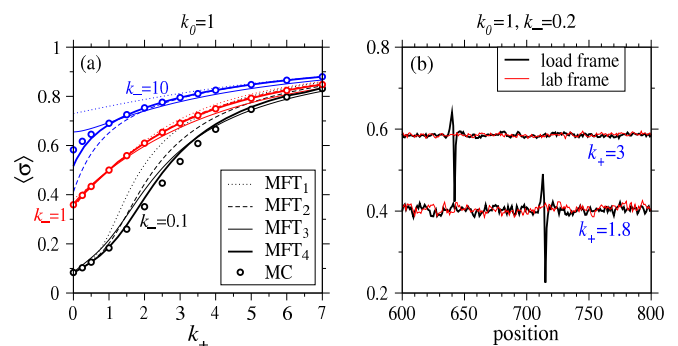


FIG. 2: (a) Mean densities computed from finite-segment MFT and from MC simulation. The three groups of densities correspond to $k_- = 0.1, 1, 10$. Within each group, finite-segment mean field results with sizes $m = 1, 2, 3, 4$ (denoted MFT_m) are compared with results from MC simulations (open circles). (b) Density profiles (for $k_+ = 1.8, 3$) in the lab frame (thin light curves) and in a frame moving with the load particle (thick dark curves) that follows the rules indicated in Fig. 3.

Fig. 2a shows the increasing accuracy in determining $\langle \sigma \rangle$ upon using larger m (shown are $m = 1, 2, 3, 4$) in the finite-segment mean field approach. Although $m = 1$ (simple mean field theory) can give results appreciably disparate from MC simulation results, larger clusters ($m = 2, 3, 4, \dots$) significantly improve convergence to the correct mean density level. Moreover, simple MFT (Eq. 2) is exact in the symmetric, equilibrium limit $k_+ \rightarrow k_-$, where the moment equations are closed.

Now consider a lattice-associated particle that can be moved by the nonequilibrium fluctuations inherent in the substrate. Simple kinetic rules are defined in Fig. 3. Without loss of generality, we also assume that the particle does not have intrinsic fluctuations. Since its stochastic motion is caused only by the asymmetric domain walls fluctuating past it, we must determine the domain wall probability *in the frame of the moving particle*. The thick solid black curves in Fig. 2b show the

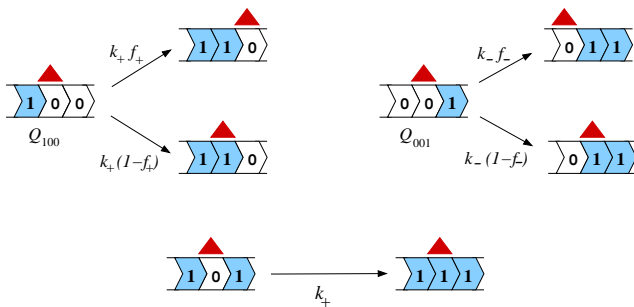


FIG. 3: The kinetic rules for domain wall-driven particle motion. A particle is pushed forward with probability f_+ whenever a $\dots 100\dots$ domain wall tries to move past it from left to right. Similarly, the particle moves backward with rate k_-f_- .

mean hydrolysis level, determined by MC simulation, in the particle frame. The particle position is arbitrary, but the hydrolysis level near it differs significantly from the uniform bulk away from the particle (or in the laboratory frame). As we follow the stochastically driven particle, the mean hydrolysis level $\langle\sigma_i\rangle$ just before (after) it is higher (lower); the particle statistically moves ahead of a domain wall, spending more time ahead of it.

The mean velocity and dispersion of the driven particle are computed from

$$V = k_+f_+Q_{100} - k_-f_-Q_{001} \quad \text{and} \quad (4)$$

$$D = k_+f_+Q_{100} + k_-f_-Q_{001},$$

where Q_{100} and Q_{001} are the steady-state probabilities that the segment of three sites centered about the driven particle is in the indicated configuration (cf. Fig. 3). In order to use mean field theory to compute Q_{100} and Q_{001} , we must use either moment equations or a finite-sized mean field transition matrix in the moving, fluctuating frame of the transported particle. In analogy to Eq. 1, we can consider the evolution equation of the first moment $\langle\sigma_\ell\rangle$ of the hydrolysis level at the site of the driven particle. In addition to the state transitions represented by rates k_\pm (hydrolysis) and k_0 (dehydration), transition terms also arise from motion of the driven particle:

$$\begin{aligned} \frac{d\langle\sigma_\ell\rangle}{dt} = & k_- - (k_- + k_0)\langle\sigma_\ell\rangle + \Delta\langle\sigma_{\ell-1}\rangle - \Delta\langle\sigma_\ell\sigma_{\ell-1}\rangle \\ & + \langle p_+(\sigma_\ell - \sigma_{\ell+1}) \rangle - \langle p_-(\sigma_\ell - \sigma_{\ell-1}) \rangle, \end{aligned} \quad (5)$$

where p_\pm are the effective forward and backward hopping rates of the particle. Since the particle moves only via motion of domain walls defined by Q_{100} and Q_{001} ,

$$\begin{aligned} p_+ &= k_+f_+Q_{100} = k_+f_+\sigma_{\ell-1}(1 - \sigma_\ell)(1 - \sigma_{\ell+1}) \\ p_- &= k_-f_-Q_{001} = k_-f_-(1 - \sigma_{\ell-1})(1 - \sigma_\ell)\sigma_{\ell+1}. \end{aligned} \quad (6)$$

Upon substitution of p_\pm in Eq. 6 into Eq. 5, and neglecting all correlations, we obtain a simple, single-site, moving-frame mean field approach to finding $\langle\sigma\rangle \approx \langle\sigma_\ell\rangle \approx \langle\sigma_{\ell\pm 1}\rangle$ as a root of a cubic equation. This simple mean field solution is only in qualitative agreement with MC simulations. In analogy to the finite-sized segment approach implemented through the transition matrix \mathbf{M} , we can also improve the simple moving-frame mean field theory by considering a sliding window of sites always centered about the driven particle [11]. Within these sites, the configurations are explicitly enumerated, transitions involving sliding the segment as it follows the driven particle are included, and steady-states are found. In our subsequent analyses, we use an $m = 5$ site segment that yields sufficiently accurate results for the parameters explored. Henceforth, we rescale time in units of k_0^{-1} (normalizing all rates with respect to k_0), and set $f_\pm = 1$.

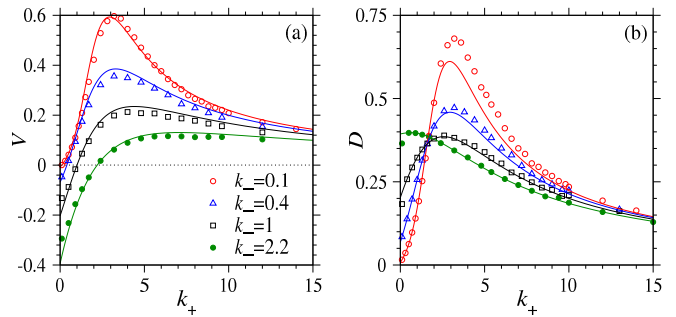


FIG. 4: (a) The mean velocity V as a function of the forward hydrolysis rate k_+ for various k_- . (b) The dispersion D for the same values of k_- . The symbols mark the values obtained from MC simulation and the solid curves are results from a 5-site finite-segment mean field approach.

Fig. 4a shows the mean velocity V derived from MC simulations and from finite-segment mean field theory applied in the moving frame of the convected particle. The agreement between MC simulation and the finite-segment MFT is quite good provided $k_- \ll 0.1$. For $k_- > k_+$, the hydrolyzed domains grow backward at a higher rate than forward, and the mean velocity $V < 0$. The velocity is positive and increases once k_+ increases past k_- . However, if k_+ becomes too large, V decreases, despite an increase in the hydrolysis asymmetry along the track. This behavior can be understood by considering Eq. 4 and Fig. 5. When both $k_\pm \ll 1$, dehydration dominates, domains are quickly dissipated, and the particle is kicked by a rare 100 domain wall as shown in Fig. 5a. Increasing values of $k_+ \gtrsim k_-$ modestly increases the asymmetry and hence V . However, if k_+ is too large, the hydrolyzed domains merge into each other, as depicted in Fig. 5c, reducing the domain wall density Q_{100} and ultimately V . Thus, there is a value of k_+ that gives an optimally combined domain wall density and nucleation asymmetry, as shown in Fig. 5b, resulting in a maximum

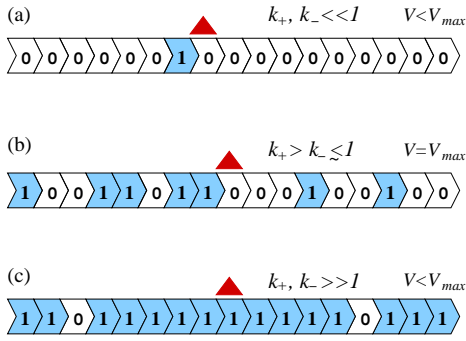


FIG. 5: The qualitative regimes that lead to maximum in mean velocity V_{max} . (a) If $k_{\pm} \ll 1$, most of the lattice remains unhydrolyzed and there are few domain walls to push the particle. (b) When $k_+ > k_-$ appreciably, but not too large to destroy domain walls, and $k_- \lesssim 1$, hydrolysis levels are intermediary, and the mean velocity is maximal. (c) For k_+ or k_- extremely large, the hydrolyzed domains coalesce, diminishing the number of domain walls. Even though the rate k_+ is large, the quantity $k_+ Q_{100}$ slowly diminishes.

mean velocity V_{max} .

For all values of k_- , an extremely large k_+ will ultimately decrease the particle velocity. Although $\Delta = k_+ - k_-$ might be large, Q_{100} decreases sufficiently that V decreases. The decrease of the mean velocity V in the $k_+ \rightarrow \infty$ limit can be determined by considering a “virial” approximation where only transitions among 111, 110, 101, and 100 need be considered. Nearly all sites are hydrolyzed and we use $s \approx 1$ in the mean field approximations. Since 100 configurations along the lattice are rare and spaced far apart, we can consider each triplet of sites as independent and find $Q_{100} \approx 2(k_0/k_+)^2 + O(k_+^{-3})$. Therefore, $V \sim 2f_+k_0^2/k_+$ as $k_+ \rightarrow \infty$.

Fig. 4b shows that the driven particle dispersion is maximal near the maximum $|V|$. This is a property of particles with no intrinsic hopping that move stochastically only when they are driven by domain walls.

In Fig. 6 we explore V_{max} and the value of k_+ that yields V_{max} (designated k_+^*) as functions of k_- . We find V_{max} and k_+^* by accurately fitting the MC simulations of V in Fig. 4 with Padé approximants and indicate these optimum values in Fig. 6 with open circles. For large k_- , the hydrolysis level is high and domain merging prevails throughout the lattice (Fig. 5c), requiring ever-higher k_+^* to arrive at a V_{max} that is smaller. Lowering k_- to intermediate values increases both the asymmetry $k_+ - k_-$ and delays the onset of domain merging, giving rise to larger V_{max} at smaller values of k_+^* . However, for $k_- \lesssim 0.1$, the hydrolyzed fraction and the onset of domain merging become insensitive to k_- and the optimal value of k_+ asymptotically approaches $k_+^* \approx 3.3$. The $m = 5$ finite-segment MFT results are plotted as solid curves and for $k_- > 0.1$ are in close agreement with those from MC simulations. Note that for the case $k_- \rightarrow 0$ before the

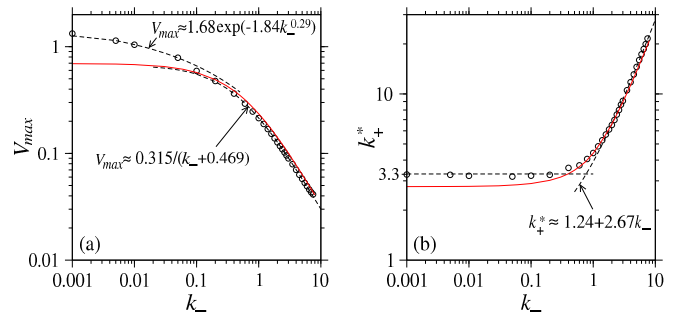


FIG. 6: (a) The maximum mean velocity V_{max} attainable and (b) the value k_+^* that yields this maximum velocity for given k_- . Results derived from MC simulation (circles) and 5-site finite-segment MFT (solid curves) compare favorably. The dashed curves are numerical fits to the MC simulation data given by Eqs. 7.

system size $N \rightarrow \infty$, $\sigma_i = 0 \forall i$ is an absorbing but unstable condition accessible only by large deviations from the stable steady-state that are exponentially unlikely in the system size. Nonetheless, for a large system a well defined steady-state can be found and V_{max} and k_+^* can be accurately fit using

$$V_{max} \approx \frac{0.315}{k_- + 0.469} \quad (7)$$

$$k_+^* \approx 1.24 + 2.67k_-, \quad k_- > 1,$$

and $V_{max} \approx 1.68 \exp(-1.84k_-^{0.29})$, $k_+^* \approx 3.3$ for $k_- < 0.1$. These expressions are plotted as dashed curves in Fig. 6 and provide accurate, universal approximations on the maximum velocity possible V_{max} as a function of k_- , and the value of k_+^* required for maximal particle velocity, for each k_- .

In summary, we have presented a paradigm for substrate-driven particle motion which has been a relatively understudied mode of subcellular transport. Our model captures the salient aspects of hydrolysis waves and exhibits rich transport behavior. Specifically, we find short-ranged state correlations, allowing us to accurately compute nonequilibrium steady-state particle velocities. For fixed backward hydrolysis rate k_- , the velocities show a maximum as a function of the forward hydrolysis rate k_+ . The value k_+^* approaches its minimum near ~ 3.3 when $k_- \lesssim 0.2$. The maximum velocities and the associated rates can be accurately described by the simple universal fitting equations 7.

Additional details such as slippage ($f_{\pm} < 1$) and an external load can be readily implemented. A load on the particle would bias the motion of the motor backwards and impart a negative drift velocity in addition to that shown in Fig. 4a. The force-velocity relationship follows directly from the functional form of the force-dependent drift.

The authors acknowledge support from the NSF (DMS-0349195) and the NIH (K25-AI058672).

-
- [1] A. B. Kolomeisky and M. E. Fisher, *Annu. Rev. Phys. Chem.*, **58**, 675-695, (2007).
 - [2] S. Saffarian, I. E. Collier, B. L. Marmer, E. L. Elson, and G. Goldberg, *Science*, **306**, 108-111, (2004).
 - [3] S. Saffarian, H. Qian, I. Collier, E. Elson, and G. Goldberg, *Phys. Rev. E* **73**, 041909, (2006).
 - [4] J. Mai, I. M. Sokolov, and A. Blumen, *Phys. Rev. E*, **64**, 011102, (2001).
 - [5] T. Antal and P. L. Krapivsky, *Phys. Rev. E* **72**, 046104, (2005).
 - [6] A. Yu. Morozov, E. Pronina, A. B. Kolomeisky, and M. N. Artyomov, *Phys. Rev. E*, **75**, 031910, (2006).
 - [7] K. Klapstein and R. Bruinsma, *J. Biol. Chem.*, **275**, 16073-16083, (2000).
 - [8] G. Schütz and E. Domany, *J. Stat. Phys.*, **72**, 277-296, (1993).
 - [9] B. Derrida and M. R. Evans, *J. Physique I*, **3**, 11-322, (1993).
 - [10] T. Chou and G. Lakatos, *Phys. Rev. Lett.*, **93**, 198101, (2004).
 - [11] S. A. Nowak, P. Fok, and T. Chou, Submitted to PRE, (2007).